Available online at www.sciencedirect.com

SciVerse ScienceDirect

Proceedings of the Combustion Institute 34 (2013) 881–886

Proceedings of the Combustion Institute

www.elsevier.com/locate/proci

Effect of pressure on structure and extinction of near-limit hydrogen counterflow diffusion flames

U. Niemann *, K. Seshadri, F.A. Williams

University of California, San Diego, Department of Mechanical and Aerospace Engineering, 9500 Gilman Drive, La Jolla, CA 92093-0411, USA

Available online 19 July 2012

Abstract

Results of measurements of critical conditions for extinction and of temperature profiles in counterflow diffusion flames are reported. The fuel was a hydrogen–nitrogen mixture with 14 mole percent hydrogen, and the oxidizer was air. Pressures ranged from 0.1 MPa to 1.5 MPa; measurements were made in a facility especially constructed for carrying out counterflow combustion experiments at high pressures. With increasing pressure, the strain rate at extinction first increases and then decreases, in qualitative agreement with predictions, but there are observable quantitative differences. Temperature profiles, obtained employing an R-type thermocouple at a fixed strain rate of 100/s, agree well with predictions, within experimental uncertainty. The results may help to improve knowledge of underlying chemical-kinetic and transport parameters at elevated pressures.

Keywords: Hydrogen; High pressure; Counterflow; Diffusion flame; Extinction

1. Introduction

Hydrogen combustion is of interest, not only because burning it directly in engines is one attractive way to make use of hydrogen as an energy carrier, but also because of safety issues associated with the relative ease with which it can be ignited. Moreover, the oxidation chemistry of hydrogen is essential to the combustion chemistry of all practical fuels, from hydrocarbons through alcohols to carbon monoxide, and possibly more so in applications involving hydrogen addition. For these reasons, the associated chemical kinetics and transport properties have been studied extensively for hydrogen. Many different sources of chemical-kinetic and transport parameters for hydrogen combustion are now available. Experimental tests of predictions derived from these different sets of parameters for various kinds of combustion processes are important for distinguishing between the different predictions and for establishing ranges of uncertainty, thereby possibly ultimately leading to improved values of parameters. New experimental results are reported here that can be used to test predictions of hydrogen combustion.

In significant respects, autoignition and flames constitute two different types of combustion processes for testing predictions. Ignition experiments, as in shock tubes, strive for homogeneous mixtures, so that transport properties are irrelevant, and radicals are not present initially, so that radical generation chemistry strongly affect the results. This applies also for detonations, as well as for initiation processes such as those in HCCI engines. Flames,

* Corresponding author.
E-mail address: uniemann@ucsd.edu (U. Niemann).

1540-7489/$ - see front matter © 2012 The Combustion Institute. Published by Elsevier Inc. All rights reserved.
http://dx.doi.org/10.1016/j.proci.2012.06.145

on the other hand, are strongly influenced by molecular transport processes, but, since radicals are already present in the hot reaction zones of flames, radical production is less important, leading to differences in the dominant chemical-kinetic steps. In this context, flames include premixed, partially premixed and diffusion flames. The present study concerns diffusion flames, specifically in a counterflow configuration, but the results may be expected to have a bearing on other combustion processes in this second category.

At least 20 shock-tube studies of hydrogen–oxygen ignition processes have been reported, extending back more than 50 years [1]. These studies have spanned a wide range of experimental conditions, with pressures ranging from less than 0.02 atm [2] to more than 80 atm [3]. In contrast, the range of conditions of existing experiments with flames is much narrower. Most of the counterflow diffusion-flame experiments, for example, have been performed at 1 atm, although some measurements have been made down to 0.5 atm [4]. No such measurements have been reported for pressures above 1 atm, although hydrogen combustion at elevated pressures is of considerable interest, for example in connection with engine application. In the present work, a newly developed high-pressure counterflow combustion facility is employed to investigate hydrogen flame structures and extinction conditions at pressures from 1 atm to 15 atm. The experimental results are compared with predictions of different chemical-kinetic mechanisms, to help to assess the uncertainties that may arise at elevated pressures.

2. Experimental conditions

Figure 1 is a schematic illustration of the counterflow configuration. Fuel mixed with nitrogen is injected from the fuel duct, and air is injected from the oxidizer duct. The reactant streams flow toward a stagnation plane. The momentum of the two streams is approximately balanced to maintain the stagnation plane at the center of the two boundaries. The mole fraction of fuel, temperature, and component of the flow velocity normal to the stagnation plane at the fuel boundary are denoted by $X_{F,1}$, T_1, and V_1, respectively. The mole fraction of oxygen, temperature, and component of the flow velocity normal to the stagnation plane at the oxidizer boundary are denoted by $X_{O_2,2}$, T_2, and V_2, respectively. The distance between the fuel boundary and the oxidizer boundary is denoted by L. Experiments were conducted with $X_{F,1} = 0.14, X_{O_2,2} = 0.21$ and $T_1 = T_2 = 298$ K, resulting in a stoichiometric mixture fraction of $Z_{st} = 0.717$, given by

$$Z_{st} = \left[1 + \frac{\nu Y_{F,1}}{Y_{O_2,2}}\right]^{-1} \tag{1}$$

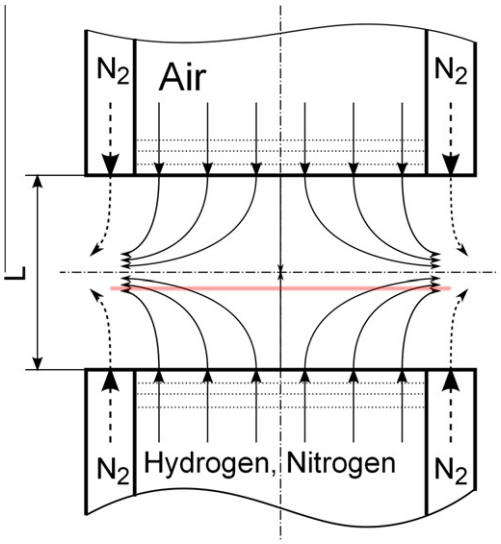

Fig. 1. Schematic illustration of the counterflow flow field.

with $Y_{F,1}$ and $Y_{O_2,2}$ as the corresponding fuel and oxygen mass fractions and ν the stoichiometric air-to-fuel mass ratio.

The experiment is designed to conform with self-similar axisymmteric channel flow with plug-flow boundary conditions [5]. In this flow, the value of the strain rate, defined as the normal gradient of the normal component of the flow velocity, changes from the fuel boundary to the oxidizer boundary. In the absence of the boundary-layer displacement effect of the flame, the characteristic local strain rate on the fuel side of the stagnation plane, a_1, would be given by [5]

$$a_1 = \frac{2|V_1|}{L}\left(1 + \frac{|V_2|\sqrt{\rho_2}}{|V_1|\sqrt{\rho_1}}\right). \tag{2}$$

Here ρ_1 and ρ_2 represent the densities of the mixture at the fuel boundary and at the oxidizer boundary, respectively. Eq. (2) is obtained from an asymptotic analysis in which the Reynolds numbers of the laminar flow at the boundaries are presumed to be large [5]. In the present experiments, these Reynolds numbers ranged from 200 to 2800. This equation, or, alternatively, the corresponding equation for the oxidizer-side strain rate, involves only known, experimentally adjustable quantities and therefore provides a convenient basis for comparison of experimental and computational results, irrespective of the strength of the boundary-layer effects, which are appreciable. A momentum balance gives $\rho_1 V_1^2 = \rho_2 V_2^2$, whence (2) becomes $a_1 = 4V_1/L$.

The inner diameter of the fuel and oxidizer ducts of the counterflow burner is 20 mm, and the separation distance between the ducts $L = 10$ mm.

Gaseous fuel mixed with nitrogen is injected from the bottom duct and air form the top. Fine wire screens are placed at the duct exits to make the tangential component of the flow velocity negligibly small there, consistent with the analysis. The ducts are surrounded by annular ducts that provide a nitrogen curtain to minimize the influence of ambient air on the reaction zone. The accuracies of the measured values of the volumetric flow rates are expected to be better than ±1%. The velocities of the reactants at the duct exits, V_1 and V_2, are calculated as the ratio of the measured volumetric flow rates of the reactants and the cross-sectional area of the ducts.

The thermocouple employed for temperature measurements is a R-type thermocouple with a wire diameter of 75 μm and a bead size of 150 μm. A hafnia coating was applied to the thermocouple to prevent catalytic surface reactions. Measured temperatures were corrected taking into consideration the radiative heat losses from the thermocouple surface.

3. Temperature profiles

Figure 2 compares measured and predicted temperature profiles at four different elevated pressures. The computations employed the San Diego mechanism along with the associated thermodynamic and transport data that can be downloaded from the web [6]. They were performed using the computer program OpenSMOKE, developed in Milan [7,8]. The code employs mixture-averaged diffusion coefficients for various species and includes radiative heat loss and thermal (Soret) diffusion. The Soret effect is especially important for calculations involving atomic and molecular hydrogen in highly diluted hydrogen flames. This effect enhances the diffusion of H and H_2 into the reaction zone, thus impacting predicted flame structures and extinction limits significantly. Discretization of differential equations is carried out using conventional finite-differencing techniques for non-uniform mesh spacing. Increasing pressure reduces the thickness of the thermal mixing layer of a strained diffusion flame. To account for the resulting strong gradients within the computational domain, dynamical adaptive meshing techniques are used. Standard calculations employ 300 grid points. Details of the computational procedure used to obtain the critical conditions of extinction have been described previously [9].

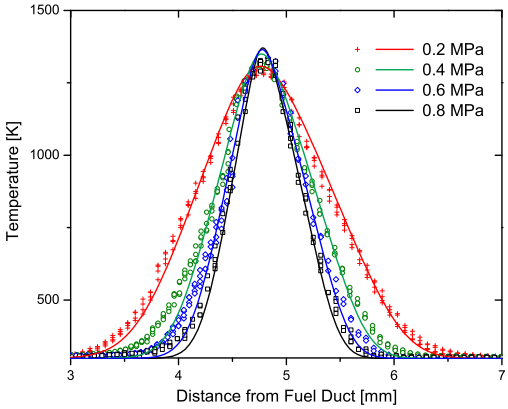

Fig. 2. Profiles of temperature as a function of distance from the fuel boundary at pressures, p, of 0.2, 0.4, 0.6 and 0.8 MPa. The strain rate is $a_1 = 100$ 1/s, and the stoichiometric mixture fraction is $Z_{St} = 0.717$ The figure shows temperature profiles corrected for radiative heat losses. The symbols represent experimental data, and the solid curves represent predictions obtained using the San Diego mechanism.

Figure 2 exhibits good general agreement between the measurements and predictions. As is expected from the value of the stoichiometric mixture fraction being greater than 0.5, the peak temperature occurs on the fuel side of the mid point between the two duct exits, at a distance less than 5 mm from the fuel boundary. The predictions and measurements are in excellent agreement in regions where the temperature profiles are nearly linear. n such regions, the finite size of the thermocouple has relatively little effect on the measurements because contributions from higher and lower temperatures tend to cancel. In regions of high curvature, however, those cancellations do not occur, and the experimental temperature profile tends to be smoothed. This effect can be seen near the peak temperature and on each side near the boundary temperature in the figure. It is thus concluded that, within the accuracy with which these temperature measurements can be made, experiment and computation are in agreement. This conclusion is further emphasized in Fig. 3, which illustrated the wire and bead sizes and shows a comparison of flames at 0.4 MPa, one for $a_1 = 100$ 1/s and one for $a_1 = 360$ 1/s, just below the value at extinction. The departures from predictions near the fuel boundary are clearly seen here to exceed those near the oxidizer boundary, the higher thermal conductivity of the gas there effectively enlarging the region of influence of the finite size of the thermocouple by enhancing heat-flow contributions farther from the center of the bead. This figure also demonstrates how increasing the strain rate decreases the peak temperature, thins the profile, and moves its location closer to the stagnation plane, as expected.

In Figure 4 the maximum temperature of the reaction zone just before extinction is shown for a pressure range from 0.2 to 0.8 MPa. These measurements were made at a strain rate equal to 90% of the experimental strain rate at extinction. Experimental measurements (symbols) indicate an increase in peak temperature with an increase in

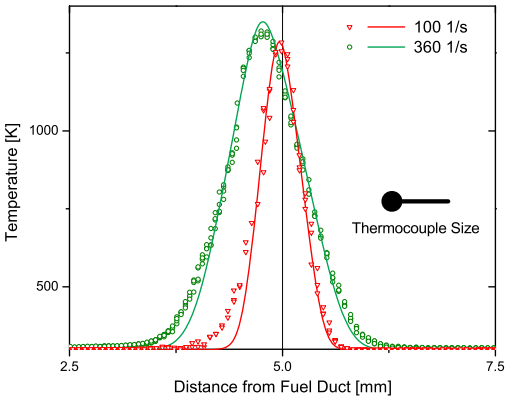

Fig. 3. Profiles of temperature as a function of distance from the fuel boundary at a pressure, p, of 0.4 MPa, for strain rates $a_1 = 100$ 1/s and $a_1 = 360$ 1/s. The figure shows temperature profiles corrected for radiative heat losses. The symbols represent experimental data, and the solid curves represent predictions obtained using the San Diego mechanism.

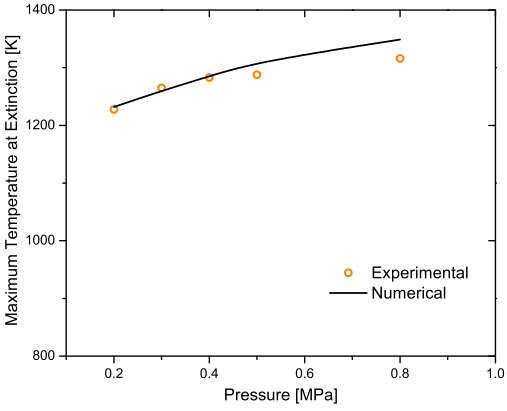

Fig. 4. The maximum temperature just before extinction. The symbols represent experimental data and the solid curve represents predictions obtained using the San Diego mechanism.

pressure, as well as a flattening trend that is also predicted by the numerical computations. The quantitative agreement between experimental measurements and numerically derived values is excellent up to a pressure of 0.4 MPa. Above 0.4 MPa the calculations predict higher flame temperatures at extinction than are measured, as may be expected from the thinning of the flame with increasing pressure, leading to increasing influences of the curvature of the temperature profile on the measurement, which will decrease the recorded temperature, as may be inferred from Fig. 3. All of the observed differences between the measurement and the prediction can thus be attributed to measurement difficulties with thermocouples. Because of the significant influence of transport properties on temperature profiles, these results thus support the validity of the transport properties employed, within experimental error. Although temperature profiles are considerably less sensitive to detailed chemical-kinetic descriptions than are profiles of concentrations of chemical species, these results also suggest that there are no gross errors in the chemistry at these elevated pressures.

4. Extinction conditions

In comparison with temperature profiles, diffusion-flame extinction conditions are much more sensitive to the chemical-kinetic descriptions. The general character of the pressure dependence of the counterflow diffusion-flame strain rate at extinction is known from earlier work. For example, as illustrated in Fig. 5, as the pressure increases, the extinction strain rate at first increases, reaches a maximum, then decreases, reaches a minimum, then begins to increase again. The reason for this type of behavior is explained by Sohn and Chung [10]. The present experiments do not extend to high enough pressures to reach the minimum of the curve, which occurs at pressures so high that they are mainly of interest only in rocket-propulsion applications. To provide a general indication of the type of agreement of the present experimental results with such predictions, the data obtained in the present study also are plotted in this figure. While both results pertain to the oxidizer-side strain rate, the computation employed potential-flow boundary conditions, while the preceding plug-flow formula is employed for the experiments. Quantitative comparisons therefore should not be expected. It can be observed that

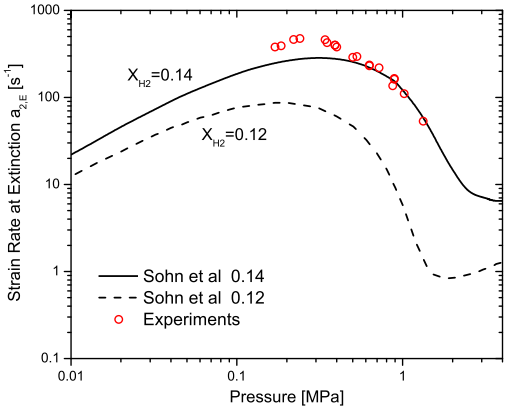

Fig. 5. The strain rate at extinction, $a_{2,E}$, for hydrogen–air diffusion flames as a function of pressure, p, at $X_{F,1} = 0.14$ and at $X_{F,1} = 0.12$, as calculated by Song and Chung [10]. Also shown for comparison are symbols representing experimental data reproduced from Fig. 6.

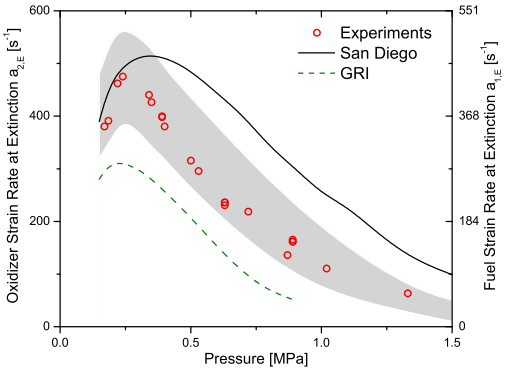

Fig. 6. The strain rate at extinction, $a_{2,E}$, for hydrogen flames as a function of pressure, p, at $X_{F,1} = 0.14$. The symbols represent experimental data, the solid curve represents predictions obtained using the San Diego mechanism [6], and the dashed curve represents predictions obtained from the GRI mechanism [11].

both results exhibit a maximum in the curve, at roughly the same value of pressure for the same composition, and that their shapes are in general agreement. No conclusion beyond that, however, can be drawn from the comparison.

Figure 6 shows the measured strain rate at extinction, $a_{1,E}$ as a function of pressure, p, at fixed $X_{F,1} = 0.14$, now on a linear rather than logarithmic pressure scale. The solid curve represents predictions obtained using the San Diego mechanism [6] and the dashed curve is obtained from the GRI mechanism [11]. Predictions of this last, well-known mechanism are shown only to illustrate that the general range of variation of predictions of different mechanisms is substantial for these extinction strain rates. The two curves shown approximately represent extremes; predictions of most other mechanisms lie between them, for the most part. See [12] for a recent re-evaluation of the hydrogen combustion chemistry.

A shaded area is provided around the experimental data to indicate the range of experimental uncertainty. The area is much wider than experimental uncertainties in measurements of pressure or of flow rates employed to calculate strain rates. The accuracy of the measured values of the volumetric flow rates, for example, is expected to be better than ±1%. Instead, extremes in the compositions of the feed streams, subject to possible experimental errors, were employed in the San Diego mechanism to calculate limiting strain-rate curves bounding the San Diego prediction, and those bounds were then lowered to bound the experimental data. In this way the shaded area provides an indication of the range of predictions that may be expected for any mechanism, subject to uncertainties in feed-stream compositions. The area narrows as the pressure increases because the uncertainties in the feed-stream compositions decrease. The boundaries of the area thus where calculated by adding the numerically derived limits to the averaged experimental data points.

It is worth pointing out that, for the conditions investigated here, the hydrogen flame is not visible, but the shadow established from its density gradients can be clearly seen. Extinction was considered to take place when this shadow suddenly disappeared. Further confirmation of extinction was provided by the observation that a rapid decrease in the exhaust-gas temperature followed immediately.

The figure shows excellent agreement between the measurements and the San Diego predictions from normal atmospheric pressure up to 0.25 MPa., well within the experimental uncertainty. This is understandable because of the previous tests of the mechanism at 0.1 MPa. At higher pressures, however, the predictions begin to fall well above the area of experimental uncertainty. The experimental data show that the highest value of $a_{1,E}$ is attained around 0.3 MPa, while the mechanism instead predicts the maximum around 0.4 MPa. And differences increase beyond that pressure. The more recent mechanism of [12] predicts oxidizer strain rates at extinction which are lower than those of the San Diego mechanism by 20–50 1/s, with a maximum at a slightly higher pressure, but above 0.5 MPa these also lie above the shaded area.

Sensitivity analysis, for example, shows those elementary reactions that give the highest values for the sensitivity coefficient with respect to T, given by the maximum value of $\partial \ln T/\partial \ln A_k$, (where A_k is the frequency factor of reaction k), as expected, are those of the chain-branching reaction $H + O_2 \rightleftharpoons O + OH$, and of the recombination step $H + O_2 + M \rightleftharpoons HO_2 + M$. The lower prediction of the mechanism of [12] may arise from the fact that their rate for the first of these steps is somewhat lower in this temperature range. It was observed that, if the chaperon efficiency for nitrogen for the latter of these steps is doubled, then the predictions of the San Diego mechanism fall right on top of the data, at all pressures tested. Such a change, however, significantly degrades agreement of predictions [1] of shock-tube ignition experiments at the lower temperatures. Therefore, at present, revisions to the mechanism are not recommended. Instead, it is simply cautioned that differences like those seen in the figure for extinction predictions should be anticipated at these elevated pressures.

5. Concluding remarks

The experimental study presented here verified that pressure has a significant effect on the extinction of non-premixed hydrogen flames. The trend of decreasing extinction strain rates with increas-

ing pressure above 0.3 MPa is strongly affected by the recombination reaction and thus by third-body efficiencies. Further study of the associated rate parameters therefore is warranted, especially, for the step $H + O_2 + M \rightleftharpoons HO_2 + M$.

Even though past theoretical findings and present chemical-kinetic mechanisms already exhibit a high level of understanding of this subject, this is the first experimental evidence that confirms the predicted non-monotonic pressure-dependent extinction behavior of non-premixed hydrogen flames. For the range of pressures investigated here, it has been found that the maximum flame temperature at extinction increases with pressure, also in agreement with previous predictions. In addition, as expected, it was confirmed experimentally that the flame thickness decreases with increasing pressure and that flames of the same composition are equally positioned independent of pressure and move towards the stagnation plane with increasing strain rate. These experimental results warrant further investigation with revised considerations of the detailed chemistry.

Acknowledgments

The authors thank Roberto Grana and Alberto Cuoci at Politecnico di Milano for valuable discussions and for granting access to the OpenSMOKE code. We thank Ryan Gehmlich for his assistance. The research at UCSD is supported by the U.S. Army Research Office, Grant # W911NF-09-1-0108 (Program Manager Dr. Ralph A. Anthenien Jr.).

References

[1] G. Del Alamo, *Theoretical Studies of Hydrogen Ignition and Droplet Combustion*, Ph.D. thesis, UCSD, 2006.
[2] R.A. Strehlow, A. Cohen, *Physics of Fluids* 5 (1962) 97–101.
[3] E. Petersen, D. Davidson, M. Rohrig, R. Hanson, in: 20th Int. Symp. on Shock Waves, 1996, pp. 941–946.
[4] P. Papas, I. Glassman, C.K. Law, *Proc. Combust. Inst.* 25 (1994) 1333–1339.
[5] K. Seshadri, F.A. Williams, *Int. J. Heat Mass Transfer* 21 (1978) 251–253.
[6] The San Diego Mechanism, 2011, available at http://combustion.ucsd.edu.
[7] A. Cuoci, A. Frassoldati, T. Faravelli, E. Ranzi, *Proc. Combust. Inst.* 32 (2008) 1335–1342.
[8] A. Cuoci, A. Frassoldati, T. Faravelli, E. Ranzi, *Combust. Sci. Technol.* 180 (2008) 767–784.
[9] K. Seshadri, A. Frassoldati, A. Cuoci, et al., *Combust. Theory Modell.* (2011) 1–15.
[10] C.H. Sohn, S.H. Chung, *Combust. Flame* 121 (2000) 288–300.
[11] GRI-Mechanism 3.0, 1999, available at http://www.me.berkeley.edu/gri_mech/.
[12] M. Burke, M. Chaos, Y. Ju, F. Dryer, S. Klippenstein, *Int. J. Chem. Kinet.* 44 (2012) 444–474.